Materials Science and Engineering A 528 (2011) 3545–3555

Contents lists available at ScienceDirect

Materials Science and Engineering A

journal homepage: www.elsevier.com/locate/msea

Effect of annealing on the microstructure and mechanical properties of cold rolled Fe–24Mn–3Al–2Si–1Ni–0.06C TWIP steel

Dagoberto B. Santos [a], Ahmed A. Saleh [b,*], Azdiar A. Gazder [b], Andrew Carman [b], Dayanna M. Duarte [a], Érica A.S. Ribeiro [a], Berenice M. Gonzalez [a], Elena V. Pereloma [b]

[a] Metallurgical and Materials Engineering Department, Federal University of Minas Gerais, Belo Horizonte, MG 30901-270, Brazil
[b] School of Mechanical, Materials and Mechatronic Engineering, University of Wollongong, New South Wales 2522, Australia

ARTICLE INFO

Article history:
Received 3 June 2010
Received in revised form 3 November 2010
Accepted 18 January 2011
Available online 26 January 2011

Keywords:
TWIP
Rolling
Recrystallisation
Twinning
Transmission electron microscopy (TEM)
Tension
Mechanical properties

ABSTRACT

Fe–24Mn–3Al–2Si–1Ni–0.06C TWinning Induced Plasticity (TWIP) steel was 42% cold-rolled and isochronally annealed at temperatures between 600 and 850 °C. Optical, secondary and transmission electron microscopy found that a majority of as cold-rolled grains contain a large fraction of primary twin densities and a smaller fraction of secondary twins. Partially recrystallised microstructures comprise a mix of recrystallised grains and annealing twins as well as remanent deformed grains with heavy dislocation substructures and deformation twins. Both deformation and annealing twins follow the $\{1\,1\,1\}\langle 1\,1\,2\rangle$ relationship. All partially recrystallised samples exhibited four work hardening regions and a decreasing twinning onset stress with greater percentage softening. A modification to the Hollomon–Ludwigson scheme is suggested to empirically account for the effect of strain on microstructural refinement.

1. Introduction

TWinning Induced Plasticity (TWIP) steels containing 25–35 wt% Mn with small additions of Al, and Si have been developed as a promising material for automotive applications [1,2]. The high Mn content stabilises austenite at room temperature and produces a single phase face centred cubic (fcc) steel with low stacking fault energy (SFE) between 15 and 40 mJ/m^2. TWIP steels are characterised by high strain hardening rates leading to ultimate tensile strengths of 600–1000 MPa and total elongations exceeding 50%. The achievement of this combination of mechanical properties challenges the conventional perception of an inverse relationship between strength and ductility and occurs mainly via the lowered SFE producing substantial twinning during plastic deformation.

To date, studies on TWIP steels have largely focused on deformation mechanisms [1–4] with few investigations on its recrystallisation behaviour [5–7]. Precise control of post-deformation annealing treatments affects the final mechanical properties by: (i) decreasing the defect/dislocation density in the cold-worked material and (ii) controlling the final microstructure in terms of grain morphology and bulk crystallographic texture [8]. Previous work on a Fe–22Mn–C TWIP steel [5–7] reported a high density of nucleation sites yielding fast recrystallisation kinetics and a fine grained microstructure of ~1–5 μm. It was shown that grain refinement either by increasing the rolling reduction or decreasing the annealing temperature leads to higher strengths while preserving ductility [9,10]. More recently, superior strength–ductility combinations were attained via recovery treatment of cold-rolled TWIP steel by maintaining the deformed nano-twinned structure while reducing the total dislocation density [11].

The microstructure, bulk texture evolution and strain hardening behaviour of TWIP steel were also investigated during tensile loading [4,12–14]. Like other low SFE materials [15,16], the work hardening behaviour evolves with deformation such that: (i) during the elastic and early plastic stage, slip is the dominant deformation mode and is associated with a pronounced decrease in the work hardening rate. (ii) Upon reaching the stress required to initiate twinning, primary twins with the same orientation inside each grain proliferate; thereby increasing or holding the work hardening at a constant level. (iii) At even higher stresses, secondary twins

* Corresponding author at: School of Mechanical, Materials and Mechatronic Engineering, University of Wollongong, Room No. 105, Bldg. 8, Northfields Av., Wollongong, New South Wales 2522, Australia. Tel.: +61 4221 5493; fax: +61 4221 3662.
E-mail address: as740@uowmail.edu.au (A.A. Saleh).

0921-5093/$ – see front matter © 2011 Elsevier B.V. All rights reserved.
doi:10.1016/j.msea.2011.01.052

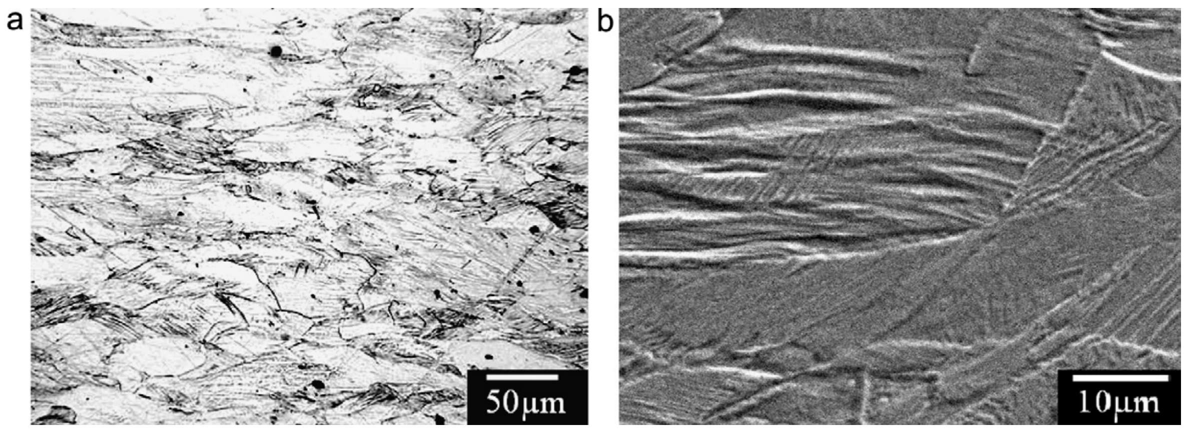

Fig. 1. Representative (a) optical and (b) secondary electron (SE) micrographs for the cold-rolled sample.

emerge and intersect the primary twins leading to extended work hardening. If primary and secondary twinning occur in sequence it results in two plateaus separated by a decreasing twinning rate [4]. However if secondary twinning occurs while primary twinning is still active, the two mechanisms overlap and a single constant or gradually decreasing extended work hardening regime is realised [13,14]. (iv) With further straining the previously formed twins hinder the production of new twins thereby decreasing the work hardening rate. This could occur as an intermediate stage between primary and secondary twinning or during the final stages of deformation. It is emphasised that the manifestation and relative extent of each of the aforementioned work hardening regions depends on several factors such as the SFE, grain size and crystallographic orientation [4,10,15–17].

Along with experimental characterisation of the work hardening, physical models that correlate bulk mechanical behaviour with the evolution of deformation twinning have been developed. TWIP-effect models are primarily based on the dynamic Hall–Petch approach [18,19] such that twin boundaries are considered to be similar to grain boundaries and act as obstacles to glide by reducing the mean free path of dislocations. The modelling scheme was further extended by including the Bauschinger effect contribution to the strain hardening due to the existence of internal micro-stresses between twins and the parent matrix [9,20].

As an alternative to physical modelling, several empirical stress–strain relationships such as the Ludwik [21], Hollomon [22] and Swift [23] equations have been used to describe plastic deformation behaviour. For low SFE metals and alloys, Ludwigson [24] suggested a modification of the Hollomon equation that deviates from $\ln(\sigma)$ versus $\ln(\varepsilon)$ linearity at lower strains. Here σ and ε refer to true stress and strain, respectively. This deviation was ascribed to the transition from planar slip at lower strains into cross slip at higher strains. Only limited attention has been directed at examining the applicability of such empirical equations and investigating the quality of fit in TWIP steel. To this end, Jin and Lee [12] preferred the modified Crussard–Jaoul (C–J) analysis [25] based on the Swift equation to delineate the work hardening stages in a Fe–18Mn–0.6C–1.5Al TWIP steel. On the other hand, Dini et al. [14] analysed the work hardening behaviour of Fe–31Mn–3Al–3Si TWIP steel with different grain sizes using the C–J analysis [26,27] based on the Ludwik equation.

The current work investigates microstructure evolution and its concurrent effect on the mechanical properties of a cold-rolled and isochronally annealed TWIP steel. The applicability of the Holloman and Ludwigson empirical relations to describe the flow curve is examined and a further modification to the Hollomon equation is also suggested.

2. Experimental procedure

TWIP steel with a nominal composition of 24Mn–3Al–2Si–1Ni–0.06C wt.% was cast in a PowerTrak 250-10 R Inductotherm™ induction furnace with fusion and pouring performed at 1558 and 1510 °C, respectively. The 300 mm × 200 mm × 30 mm cast plate was machined into 100 mm × 80 mm × 30 mm strips and then austenitised at 1100 °C for 2 h. The strips were re-heated to 1100 °C and hot-rolled in four passes with ~17% reduction per pass to achieve a total thickness reduction of 52%. Surface oxides and scales were then removed by machining. Following this, cold-rolling (CR) was undertaken in 11 passes at ~4.8% reduction per pass to a final thickness reduction of 42%; thereby achieving a final strip thickness of 7.3 mm.

30 mm × 10 mm × 7.3 mm samples were cut from the cold-rolled strip and isochronally annealed at the temperatures between 600 and 850 °C. The heat treatment included 240 s of heating to stable temperature followed by 300 s of soaking time and immediate water quenching. Average Vickers microhardness was determined from twenty measurements per sample using a 500 g load on a Leitz RZD-DO microhardness tester.

Microstructure characterisation via optical microscopy (OM) and secondary electron (SE) imaging was conducted on transverse direction (TD) sections from the middle of the sample cross-section. The sections were polished up to 1 μm and etched with 2% Nital solution. In accordance with the ASTM E112 standard, the austenite grain size was estimated from the SE micrographs as the square root of the average area of a minimum two hundred grains per sample.

For transmission electron microscopy (TEM), normal direction (ND) sections of ~200–300 μm thickness were initially sliced using a Struers Accutom-50 at a cutting speed of 0.01 mm min^{-1}. Thereafter 3 mm diameter disks were punched out and ground down in two steps to ~120 μm using 1200 grit and then to ~100 μm thickness with 2400 grit SiC paper. Each TEM disk was electrolytically thinned using a twin-jet Struers Tenupol-5 electropolisher in a solution of 95% methanol and 5% perchloric acid. Polishing conditions were maintained at 30 V, ~150 mA at −25 °C for all conditions. Bright- and dark-field imaging and selected area diffraction (SAD) were performed on a JEOL JEM 2011 TEM operating at 200 kV and equipped with an Olympus MegaView-II digital imaging system.

Round tensile samples of 25 mm gage length and 4 mm diameter were machined from all samples parallel to the rolling direction. Room temperature tensile tests were performed on an electro-mechanical Instron 5582 at a constant speed of 1.7 mm min^{-1}; which corresponds to an initial strain rate of 1.03×10^{-3} s^{-1}. Rational polynomial functions were used to fit the true stress–strain curves using TableCurve-2D in order to estimate the work hardening via program-based calculations in MATLAB.